Preprint
UCRL-JC-135910

Hydrogen at High Pressure and Temperature

W. J. Nellis

This article was submitted to International Conference on High Pressure Science and Technology, Honolulu, HI, July 25-30, 1999

September 9, 1999

U.S. Department of Energy

Lawrence
Livermore
National
Laboratory

Hydrogen at High Pressures and Temperatures

W. J. Nellis
Lawrence Livermore National Laboratory, University of California,
Livermore, CA 94550, USA

Hydrogen at high pressures and temperatures is challenging scientifically and has many real and potential applications. Minumum metallic conductivity of fluid hydrogen is observed at 140 GPa and 2600 K, based on electrical conductivity measurements to 180 GPa (1.8 Mbar), tenfold compression, and 3000 K obtained dynamically with a two-stage light-gas gun. Conditions up to 300 GPa, sixfold compression, and 30,000 K have been achieved in laser-driven Hugoniot experiments. Implications of these results for the interior of Jupiter, inertial confinement fusion, and possible uses of metastable solid hydrogen, if the metallic fluid could be quenched from high pressure, are discussed.
[Metallic hydrogen, laser compression, Jovian interior, inertial confinement fusion, metastable metallic hydrogen]

1. Introduction

Hydrogen is one the most challenging elements in the Periodic Table because of its large zero-point motions, the absence of core electrons in the atom, its strong tendency for atoms to pair, and its quantum nature at temperatures not normally thought of as low. For these reasons the metallization of hydrogen has been an outstanding issue in condensed matter physics for over one hundred years. The cosmological abundance of hydrogen is ~90 at.%, much of it in the dense fluid phase in giant planets with magnetic fields in this and other solar systems. Thus, the electrical conductivity and equation of state are important for planetary science. Hydrogen is important technologically. As a mixture of deuterium and tritium (DT), hydrogen is the fuel in inertial confinement fusion (ICF). The National Ignition Facility (NIF) is a giant laser now being built for ICF at the Lawrence Livermore National Laboratory at an estimated cost of $1 B. It is important to determine the equation of state of fluid hydrogen at high pressures and temperatures to design fusion capsules which will maximize nuclear-fusion energy yield when NIF is completed in the next few years. Metastable solid metallic hydrogen, if it could be stabilized on release of pressure, might be novel scientifically, including a possible room-temperature superconductor [1], and might have other technological applications [2].

The situation in the 100 GPa range is illustrated in Fig. 1, which shows pressures versus molar densities in various temperature regimes. These include the theoretical results for the hcp solid phase at 0 K [3], states of the hcp solid at 300 K determined in a diamond anvil cell with x-ray diffraction [4], fluid states at 2000-3000 K generated with a two-stage gun in electrical conductivity experiments [5], and single-shock Hugoniot equation-of-state data achieved with a giant laser [6]. The results at ~10^2 K are for a quantum diatomic solid insulator. The states at ~10^3 K are for a quantum fluid [2,7]. Above 140 GPa the fluid is metallic and the electrons are highly degenerate. This fluid is expected to consist primarily of transient dimers, monomers, and probably some higher order clusters [8,9]. The dimers exist in quantized vibrational states for a time comparable

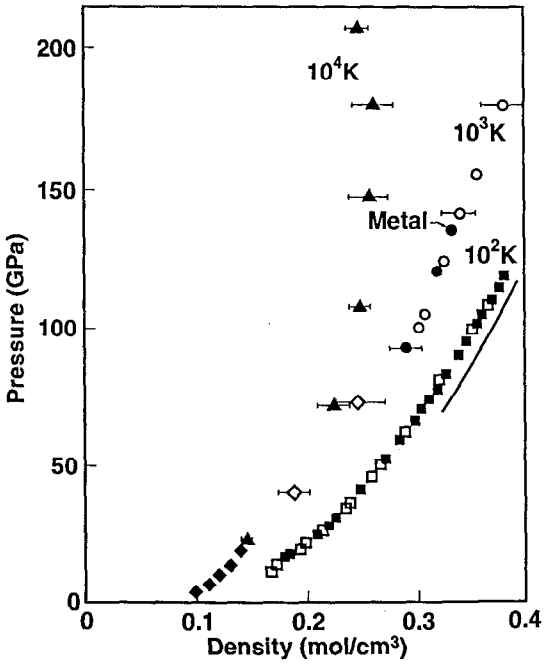

Fig. 1. Pressure-volume curves: theoretical 0-K isotherm of hcp-phase H_2 (solid curve) [3]; hcp solid phase in diamond anvil cell at 300 K of H_2 (open sqares) and D_2 (solid squares) [4]; fluid states in electrical conductivity experiments using two-stage gas gun for H_2 (open circles) and D_2 (solid circles) [5]; D_2 Hugoniot points obtained with laser (solid triangles) [6]; Hugoniot points obtained with gas gun under single shock (solid diamonds) and double shock (open diamonds) [44].

to the vibrational period of the free molecule and protons in dimers exchange on collisions. Both electrons and protons must be treated quantum mechanically, something which is yet to be done. The results at ~10^4 K are for a fluid with degenerate electrons and classical protons [6]. This transition from diatomic insulator to conducting fluid is continuous and complex - from solid

to fluid, from insulator to metal, from diatomic to monatomic, and from quantum to classical.

Because hydrogen at high temperatures diffuses so rapidly, high-temperature experiments must be performed on short time scales. For this reason most hydrogen experiments at high pressures and temperatures have been performed under shock compression, in which experimental lifetimes are long for thermal equilibrium and fast for mass diffusion.

The purpose of this paper is to review what has been learned over the past several decades about fluid hydrogen at high pressures and temperatures and to speculate about the future.

2. Metallization of Condensed Hydrogen

The quest for metallic hydrogen has been going on for over one hundred years. Prior to 1898 many scientists expected that condensed hydrogen would be a metal at atmospheric pressure [10]. This prediction was based on the assumption that hydrogen would be a monatomic alkali metal, as the elements below hydrogen in the first column of the Periodic Table. Hydrogen was first liquified in 1898 and solidified in 1899 by James Dewar. Both these condensed phases are transparent insulators. So instead of being a monatomic alkali metal at ambient pressure, hydrogen is a diatomic insulator, as the halogens in the seventh column of the Periodic Table.

The Goldhammer-Herzfeld criterion for the density of metallization was published in 1927 [11]. It is based on the Claussius-Mossotti relation (1850) and the fact that the index of refraction becomes infinite at metallization. This criterion gives essentially the same metallization density of fluid hydrogen observed in 1996 [5,12]. In 1935 Wigner and Huntington used quantum mechanics to predict that solid H_2 at T = 0 K undergoes a first-order transformation to monatomic H at a pressure estimated to be 25 GPa, with an associated insulator-metal (IM) transition [13]. In 1960 Alder and Christian predicted that the Wigner transition would occur at 2000 GPa [14].

In 1978 Hawke et al reported that under isentropic magnetic flux compression hydrogen resistivity is 10^6 μΩcm at 200 GPa and 400 K [15]. While this resistivity is indicative of electrical conduction, it is not metallic. In 1979 Inoue et al measured an electronic bandgap of 15 eV for solid H_2 at 1 bar [16], illustrating why it is so difficult to metallize hydrogen. In 1983 Ross et al predicted that at 0 K the IM transition is in the range 300-400 GPa, based on shock compression data [17]. In the mid 1980's static high-pressure experiments by Mao, Bell, Hemley, Silvera, Ruoff and their coworkers began on hydrogen at several 10 GPa. In 1987 Pavlovskii et al reported that under isentropic magnetic flux compression hydrogen resistivity is 10^4 μΩcm at ~100 GPa and ~300 K [18], conductive but not a metal.

In 1990 Ashcroft predicted that solid H_2 at T = 0 K would dissociate into solid H and metallize at ~300 GPa [19], based on vibron data in a diamond cell [20]. Garcia et al [21] and Chacham and Louie [22] performed theoretical calculations which showed that the metallization pressure depends strongly on the orientation of the H_2 molecule in the hcp phase. Kaxiras et al showed that hcp is not the structure of metallic hydrogen because phases with lower symmetry have lower total energies, as well as larger bandgaps, than the hcp phase [23]. Optical measurements show that solid H_2 is an insulator to ~250 GPa [24-26]. Loubeyre et al performed x-ray diffraction experiments on solid H_2 and D_2 and found the hcp phase up to 120 GPa [4]. Using their measured pressure-volume curve for the molecular phase and theoretical results for the monatomic metallic solid, they estimated that the Wigner IM transition would occur at ~620 GPa. In 1998 Narayana et al observed that solid H_2 is not metallic at 340 GPa and 300 K [27].

Weir et al and Nellis et al [5,7] observed minimum metallic conductivity in fluid hydrogen at 140 GPa, ninefold compression of initial liquid-H_2 density, and ~2600 K. These conditions were achieved with a reverberating shock wave and illustrate the importance of using just enough temperature to enter the melt region at very high densities. Disorder in the fluid sufficiently lowers the metallization pressure to observe a metallic state at accessible pressures. Metallic fluid hydrogen at 3000 K is a quantum fluid, both electronically and vibrationally, because the temperature is small compared to the Fermi temperature and the ground state vibrational energy of the molecule is 3000 K, comparable to the temperature, with the first excited state at ~9000 K. Hydrogen is also in thermal equilibrium in the 100 ns lifetime of the experiment because the time between molecular collisions is 10^{-5} ns. Thus, for hydrogen at ninefold compression, 3000 K is a relatively low temperature and 100 ns is a relatively long time. Similar results were found by Fortov and coworkers [28].

2a. Conductivity Experiments With a Gas Gun

The experimental configuration is illustrated in Fig. 2. A 0.5 mm-thin layer of liquid H_2 or D_2 is compressed dynamically by a high-pressure shock wave reverberating between two stiff, electrically-insulating sapphire (single-crystal Al_2O_3) anvils, 25 mm in diameter. The two sapphire anvils are contained between two Al plates, which are part of a cryostat at 20 K. The initial temperature is cryogenic to achieve the relatively high initial density of the liquid at 0.1 MPa. The compression is initiated by a shock wave generated when a metal plate, launched by a two-stage light-gas gun at velocities up to ~7 km/s, impacts the Al plate on the left in Fig. 2. The impact shock is amplified when it is transmitted into the first sapphire anvil. The first shock pressure in the sapphire anvil is obtained with a 1% uncertainty by impedance matching the measured impactor velocity and the Hugoniots of the impactor, Al, and sapphire. The first shock pressure in the liquid is ~30 times lower than the shock incident from the sapphire. The shock then reverberates quasi-isentropically between the two anvils until the final hydrogen pressure equals the shock pressure initially

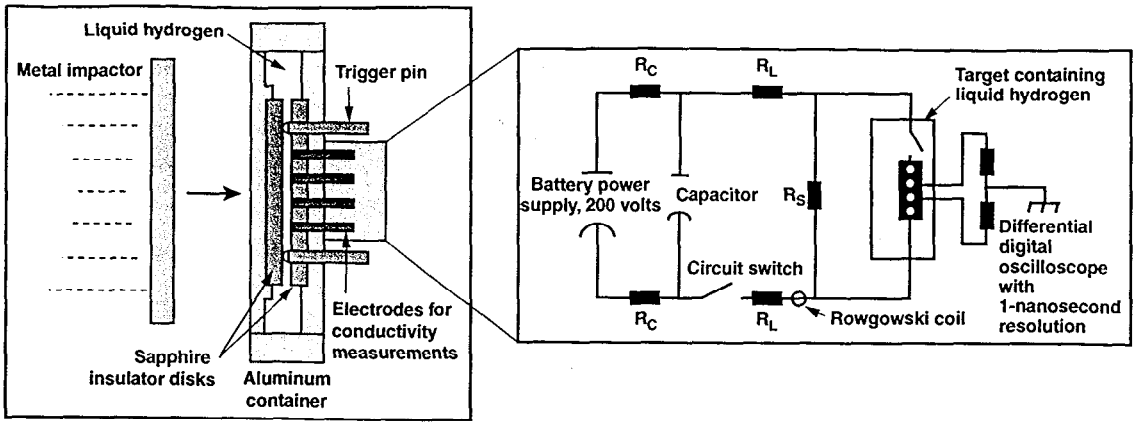

Fig. 2. Schematic of electrical conductivity experiments with two-stage gun. High shock pressures are generated by impact onto cryogenic target holder containing liquid H_2 at 20 K. For metallic phase two outer electrodes are connected to current supply and two inner electrodes are connected to fast digital oscilloscopes [7].

incident from the sapphire, as illustrated in Fig. 3, which shows the calculated pressure history at the midpoint of the hydrogen layer. The pressure-density (P-D) states achieved by shock reverberation are illustrated in Fig. 4, relative to the 0-K isotherm and the single-shock Hugoniot. The final temperature produced by a reverberating shock is about 1/10 what it would be for a single shock to the same pressure. Figure 4 also shows

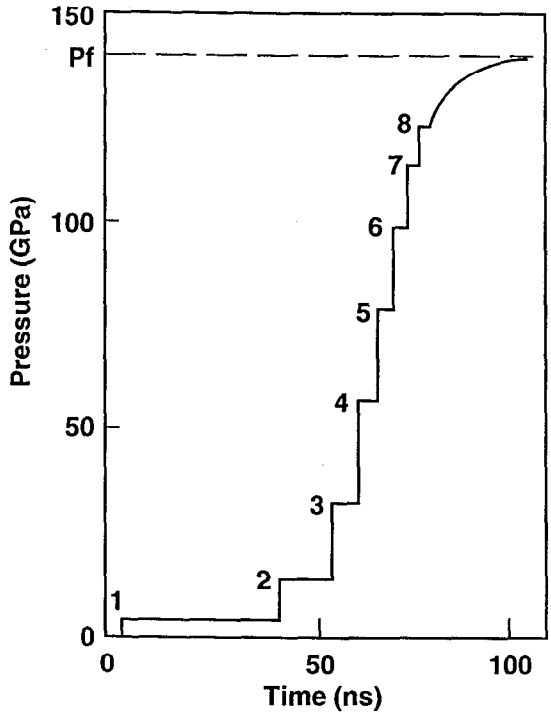

Fig. 3. Calculated pressure history at midpoint of liquid H_2 sample in Fig. 2 for experiment at 140 GPa. Step increases in pressure are caused by shock wave reverberating between two sapphire disks in Fig. 2 [7].

that states achieved by shock reverberation are relatively close to the 0 K isotherm and at much higher densities than the single-shock Hugoniot. At metallization the calculated temperatures are about twice the calculated melting temperatures. While the final hydrogen pressure depends simply on shock impedance matching known quantities of solids, the calculated density and temperature depend on the hydrogen equation of state. Analysis of the experimental data shows that the density at which hydrogen reaches minimum metallic conductivity depends weakly on the assumed equation of state [7].

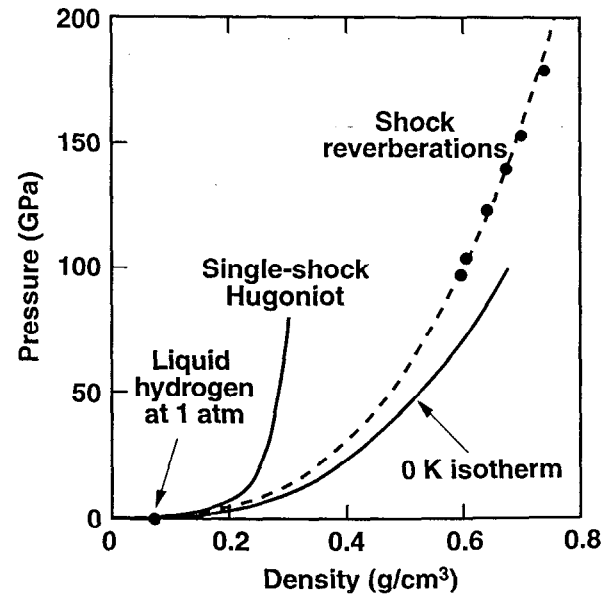

Fig. 4. Illustration of thermodynamic effect of reverberating shock wave relative to other compression paths plotted as pressure versus volume: 0-K isotherm; points reached by shock reverberation; and Hugoniot curve of single-shock compression [7].

Electrical resistance of the hydrogen sample was measured versus time by inserting electrodes through the anvil on the right in Fig. 2. H_2 or D_2 samples were used, depending on the final density and temperature desired, H_2 giving lower final temperatures than D_2. That is, because

the initial mass densities of liquid H_2 and D_2 differ by a factor of 2.4 at 20 K, the final shock-compressed densities and temperatures also differ. Thus, H_2 and D_2 were used to obtain different final densities and temperatures and not to look for a quantum-mechanical isotope effect, which does not exist at 3000 K, nor is it evident in the static P-D data at 300 K [4]. Our experimental data [5] are plotted in Fig. 5 as electrical resistivity versus pressure, P_f in Fig. 3.

The slope change at 140 GPa in Fig. 5 is indicative of the transition from a semiconducting fluid with thermal activation of electron carriers across a mobility gap to a state with the minimum conductivity of a metal. That is, the resistivity plateaus when the mobilty gap is reduced by pressure until it is filled in by fluid disorder and smeared out thermally at $E_g(D) \sim k_B T$, where $E_g(D)$ is the density-dependent mobility gap in the electronic density of states of the fluid, k_B is Boltzmann's constant, and T is temperature. At this point the system has a Fermi surface and electron scattering is strong because of disorder. $E_g(D)$ derived from fitting the data and $k_B T$ are equal at a density of 0.32 mol H_2/cm^3 and a temperature of ~2600 K (0.22 eV). At 0.32 mol H_2/cm^3

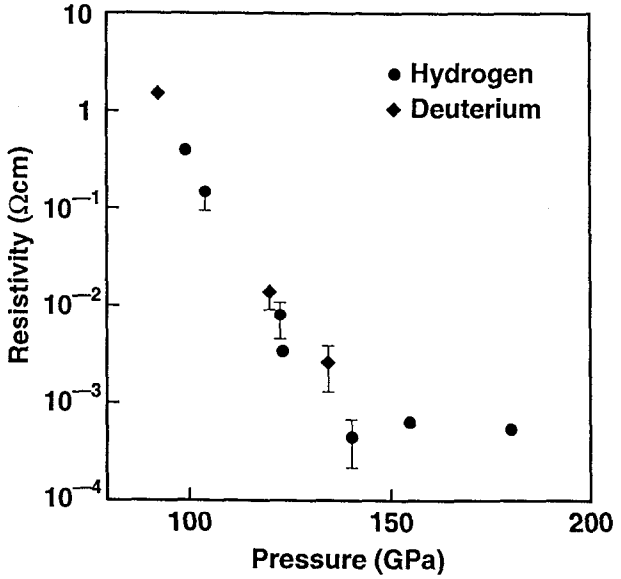

Fig. 5. Logarithm of electrical resistivity of hydrogen and deuterium versus pressure [5].

and 2600 K the calculated pressure is 120 GPa, close to 140 GPa at which the slope changes in the electrical resistivity (Fig. 5). At pressures of 140 to 180 GPa the measured hydrogen resistivity is constant within the resolution of the experiment because the minimum metallic conductivity of a disordered metal has been reached.

2b Discussion

This metallic resistivity of 500 μΩcm (or a conductivity of 2000 $(\Omega cm)^{-1}$) is essentially the same resistivity as that of the fluid alkali metals Cs and Rb at 2000 K undergoing the same nonmetal-metal transition, illustrated in Fig. 6 [29]. The minimum metallic conductivity of fluid Cs, Rb, and H is achieved at essentialy the same Mott-scaled density of $D_m^{1/3}a^* = 0.38$, where D_m is the density at metallization and a* is the radius of the peak in the charge density associated with the valence orbital; for H, $a^* = a_B$, the Bohr radius. Since the effective Bohr radius is the same for H_2 and H [7,30], the difference in the Mott-scaled density between the diatomic and monatomic states is simply a factor of $2^{1/3}$. Thus, assuming hydrogen is purely molecular H_2, rather than monatomic H, then H_2 reaches the minimum metallic conductivity at a Mott-scaled density of 0.30. Mott's preferred value is 0.25 [31].

Iodine is another diatomic element, as hydrogen, which metallizes at much lower pressure in the liquid, 3 GPa [32], than in the solid, 16 GPa [33]. The measured pressure dependences of the resistivities near metallization are very similar for iodine and hydrogen [34].

Based on Ross' bulk thermodynamic calculations, the temperatures are ~3000 K and an estimated 5% of the molecules are dissociated at metallization [5, 35]. Tight-binding molecular dynamics

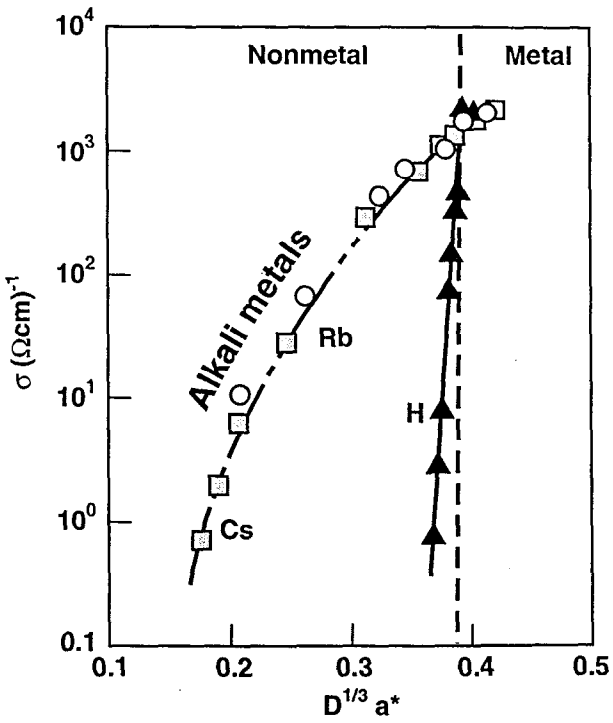

Fig. 6. Electrical conductivity of fluid Cs (squares), Rb (circles), and hydrogen (triangles) versus $D^{1/3}a^*$, where D is density and a* is effective Bohr raduius [29]. $D^{1/3}a^*$ is ratio of particle size to interparticle separation.

(TBMD) simulations also show that fluid metallic hydrogen at these temperatures is essentially molecular [36,37]. The free-electron Fermi energy of metallic fluid hydrogen, including all the electrons, is $E_F \sim 19$ ev. Since at metallization $T/T_F \sim 0.01$, metallic fluid hydrogen is degenerate, highly-condensed matter. Since the ground-state vibrational energy of H_2 is ~3000 K and the first excited state is 9000 K, most of the species are dimers,

with a few in an excited state and some dissociated; clusters also probably exist dynamically.

The measured metallic resistivity is bracketed by simple theories. The minimum electrical conductivity of a metal is given by $\sigma = 2\pi e^2/3hd$, where e is the charge of an electron, h is Planck's constant, and d is the average distance between particles supplying the electrons [31]. In this case $d = D_m^{1/3}$. D_m derived from analysis of the data is 0.32 mol H_2/cm^3 [7] and 0.30 mol H_2/cm^3 derived from the Goldhammer-Herzfeld criterion [12]. Both densities give a calculated minimum metallic conductivity which corresponds to a resistivity of 250 μΩcm, within a factor of 2 of the measured value. The slope of the mobility gap with density derived from the experimental data agrees within 50% with the predicted slope of the H_2 energy gap of the hcp phase at 0 K [7, 22], a reasonable result. At 140 GPa and temperatures in the range 1500 to 3000 K, the resistivities calculated with TBMD are 500 to 250 μΩcm [37], respectively, in good agreement with experiment. The electrical conductivity calculated with the Ziman model for diatomic metallic fluid hydrogen and a free-electron density of states is within a factor of ~10 of the measured value, also in good agreement with experiment [9].

Although metallic fluid hydrogen behaves as a relatively simple disordered metal in a time-averaged sense, the dynamics of electrons and protons are extremely complex. Below ~5000 K both electrons and protons must be treated quantum mechanically, something yet to be done. The complexity of the dynamics in this fluid is illustrated by the cinematic representation of the TBMD results, which show that the energies of translation, vibration, and rotation are comparable and that protons in dimers exchange on collisions on the timescale of a molecular vibrational period [36].

All the experimental data are continuous in density within experimental resolution and no discontinuity in density is required to explain the experimental data.

The pressure required to achieve metallization is lower in the fluid than in the ordered solid probably because orientational and crystalline phase transitions, which inhibit metallization in the ordered solid [38], do not occur in the disordered fluid. In the fluid, charge clouds on neighboring molecules and/or atoms are compressed until they overlap and electrons are delocalized; that is, a Mott transition occurs from a nonmetal to a state with minimum metallic conductivity.

Measured conductivities of water up to 180 GPa in the sample holder in Fig. 2 are an order of magnitude smaller and have the expected and substantially different pressure dependence from that of hydrogen. Protons are the principal charge carriers in water at 100 GPa pressures and several 1000 K [39,40]. In contrast, preliminary electrical conductivity measurements on liquid oxygen up to 80 GPa suggest that the conductivity is thermally activated in a semiconducting fluid. Extrapolation of this data suggests that minimum metallic conductivity will be achieved at ~100 GPa [41], as expected.

Electrical resistivities of disordered metals are similar for fluids and solids. The electrical resistivity ρ of a metal varies as $\rho \sim (n\tau)^{-1}$, where n is the density of electron charge carriers and τ is the relaxation time for electron scattering. For a metal n is essentially constant and τ is very sensitive to disorder, which can be induced by thermally activated phonons in a perfect lattice, radiation damage, or melting. The highly-ordered weak-scattering case corresponds to a large τ; the disordered strong-scattering case corresponds to a small τ. Radiation damage can cause the degree of disorder to vary continuously from the highly ordered to the totally disordered state, as illustrated for $LuRh_4B_4$ in Fig. 7 [42]. For the highly ordered crystalline case (no α damage) resistivity increases relatively rapidly with temperature-induced phonon disorder. However, α-particle induced lattice disorder increases the magnitude of resistivity and simultaneously decreases its slope with temperature, dρ/dT, until minimum metallic conductivity (~400 μΩcm) is reached; the normal-state slope dρ/dT at

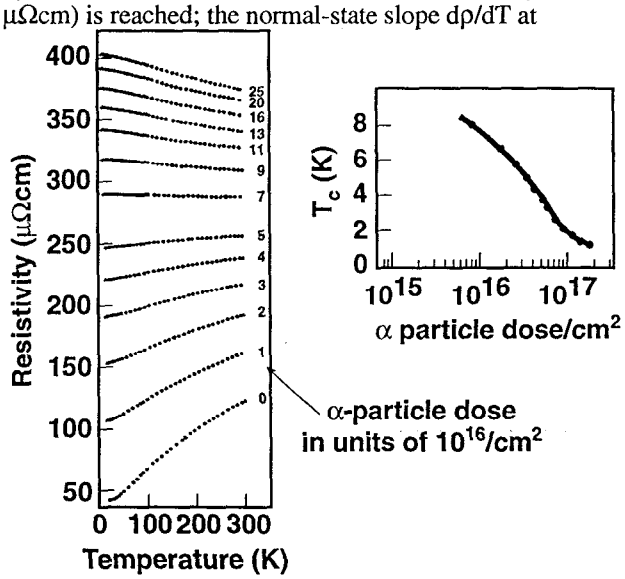

Fig. 7 Electrical resistivity of intermetallic compound $LuRh_4B_4$ versus temperature for various α-particle doses and corresponding superconducting transition temperatures, T_c, as function of α–particle dose [42].

low T is positive, zero, or negative, depending on the degree of disorder. The compounds in Fig. 7 have a wide range of crystalline disorder and all are superconducting metals. The minimum metallic conductivity of disordered $LuRh_4B_4$ (Fig. 7) is the same within the uncertainties as the minimum metallic conductivity of fluid hydrogen above 140 GPa (Fig. 5).

3. Laser-Driven Hugoniot Experiments

Hugoniot equation-of-state experiments have been conducted on liquid D_2 in the shock pressure range 20 to 200 GPa achieved with the Nova laser [6,43]. These pressures exceed by an order of magnitude the maximum single-shock Hugoniot pressure of 20 GPa generated with a two-stage gun [44]. The data are continuous in density within the resolution. The laser Hugoniot experiment is illustrated in Fig. 8. A high-

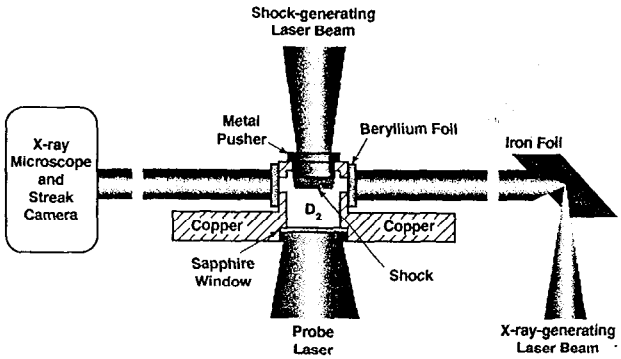

Fig. 8. Schematic of laser-driven Hugoniot experiment on liquid D_2.

intensity laser beam generates a strong shock wave in a metal plate, called a pusher. The shock transits the pusher and then shock compresses liquid D_2. A portion of the original laser beam is used to generate a soft x-ray beam by irradiation of an iron foil. This x-ray beam is used to sidelight the shock transit of the liquid D_2. That is, the soft x-ray beam is transverse to the direction of shock propagation and passes through the liquid into an x-ray microscope coupled to a streak camera. The leading edge of the shock front scatters x rays out of the field of

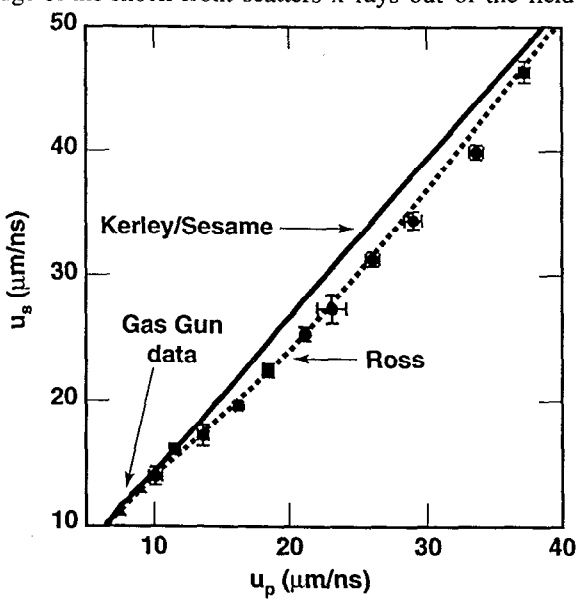

Fig. 9. Measured Hugoniot of D_2 plotted as u_s versus u_p obtained with Nova laser (solid squares) [6] and two-stage gun [44] with theoretical results of Ross [45] and of Kerley [46].

view and its position versus time, shock speed u_s, is observed as a thin dark line on the streak camera record [6]. The moving pusher absorbs the x rays. The mass, or particle, velocity u_p is equal to the velocity of the moving opaque interface between pusher and deuterium, whose motion is observed as a moving boundary of x-ray opaqueness [6]. The streak camera records show that deuterium compressions are large and that the error bars are also relatively large. These experiments are important new probes into a previously unexplored regime of pressures and temperatures.

Experimental results for D_2 are illustrated in Fig. 9, a plot of u_s versus u_p, as well as Hugoniot data taken with a gas gun and theoretical results of Ross [45] and of Kerley [46]. The latter are incorporated into the Sesame equation of state (EOS) database at Los Alamos National Laboratory. The u_s-u_p data in Fig. 9 are plotted as shock pressure P versus density D in Fig. 10. The data were converted from u_s-u_p to P-D by means of the Hugoniot equations. Because of the very high compressions, the relatively small difference between the two theories in Fig. 9 corresponds to their 50% difference in density in Fig. 10, illustrating the importance of accuracy in these experiments. Also shown in Fig. 10 are several other theoretical results [47-50]. Figure 10

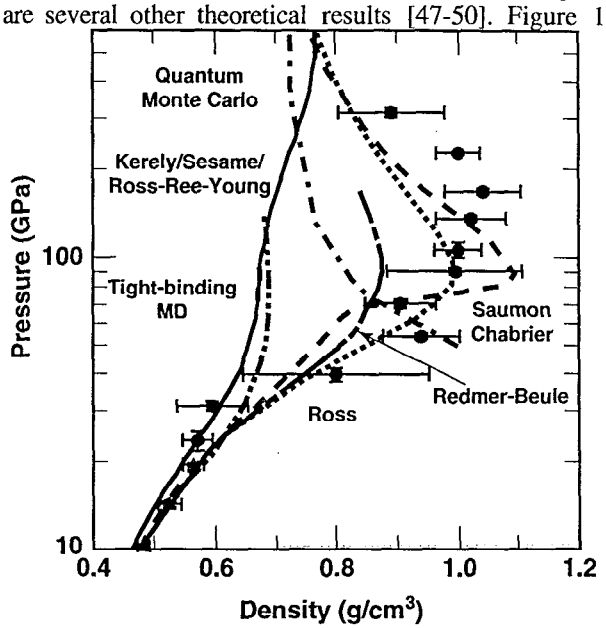

Fig. 10. Measured Hugoniot of D_2 plotted as logarithm of pressure versus mass density [6] and results of several theoretical calculations [45-50].

shows why the D_2 Hugoniot at 100 GPa pressures and eV temperatures is such an interesting scientific problem. The experiments are extremely challenging and a theoretical consensus is yet to emerge to explain the unusual experimental results. Hugoniot temperatures have also been measured at high densities [51]. Measured reflectivities of the D_2 shock front increase rapidly from ~0.1 at 20 GPa up to 0.6 above 50 GPa, indicative of a high density of electrons and a conductive state [52]. Because of the relatively high temperatures on the Hugoniot, a substantial fraction of the original dimers are dissociated into monomers. Densities, temperatures, electronic activations, and dissociation fractions on the Hugoniot are much different than in the highly condensed semiconducting and metallic fluids obtained with a reverberating shock wave, discussed in 2.

4. Scientific and Technological Applications

The importance of dense fluid hydrogen for planetary science, inertial confinement fusion, and potential technological applications are discussed below.

4a. Jupiter

Since hydrogen has a cosmological abundance of ~90 at.%, it is the main constituent of giant planets in this and other solar systems. Jupiter, for example, contains over 300 Earth masses, most of which is hydrogen. The interior is at high pressures and temperatures because of the large mass and low thermal conductivity [53, 54]. Pressure and temperature in the mantle of Jupiter range up to 300 GPa and several 1000 K and are about 4 TPa and 20,000 K at the center [55]. Hydrogen is fluid at these conditions [56]. Magnetic fields of Jovian planets are produced by the convective motion of electrically conducting hydrogen by dynamo action [57]. The magnetic field of Jupiter is that of an eccentric, tilted dipole with an admixture of higher-order multipoles. This field varies from 14 G at the north magnetic pole to 11 G at the south magnetic pole [58,59]. Thus, while the Jovian magnetic field appears to be only slightly more irregular than that of the Earth in a relative sense [58], its magnitude and its variation are ~20 and 6 times, respectively, greater than the Earth's field. These observations raise some interesting questions. For example, why is the magnitude of the Jovian magnetic field so large and asymmetric compared to that of Earth and is there a sharp core-mantle boundary in Jupiter between a molecular mantle and monatomic core, analogous to the boundary in Earth between the rocky mantle and Fe core? Answers are suggested by the continuous dissociative phase transition of H_2 to H and the presence of ~10 at.% He.

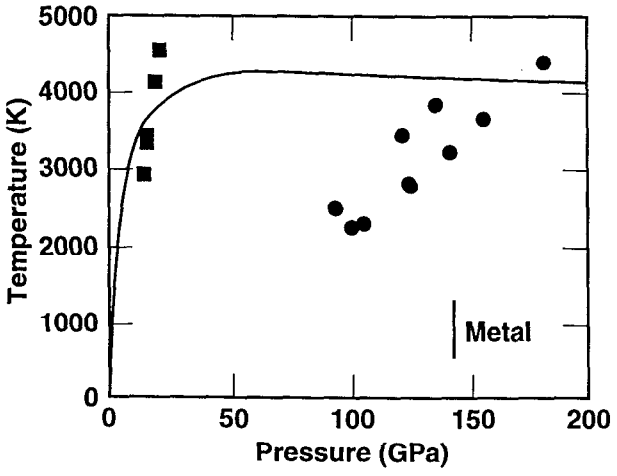

Fig. 11. Isentrope of hydrogen calculated from surface temperature of Jupiter (solid curve) [60]. Solid points are states at which electrical conductivities have been measured [7]. Mimimum metallic conductivity is reached at 140 GPa [61].

The continuous dissociative phase transition in the fluid implies that there is no sharp core-mantle boundary at a specific radius in Jupiter at which only H_2 exists at larger radii and only H exists at smaller radii. The isentrope of H_2 starting from the measured surface temperature of Jupiter (160 K) has a long plateau when plotted as temperature versus pressure [60], illustrated in Fig. 11. Temperature on this isentrope increases rapidly with pressure up to ~40 GPa. At higher pressures, the temperature is roughly constant and might even have a slight negative slope with pressure. This plateau is caused by thermal energy absorbed in molecular dissociation. Evaluation of the electrical conductivity of hydrogen along this isentrope shows that the minimum conductivity of a metal is reached at 140 GPa, which corresponds to a radius of ~0.9 R_J, where R_J is the radius of Jupiter [61]. Because the maximum electrical conductivity is reached so close to the surface, there is little radial distance in which the magnetic field can attenuate. Thus, the Jovian magnetic field is ~20 times greater than those of Saturn and Earth, because the magnetic fields of those planets are made at ~0.5 those planets' radii, much deeper than for Jupiter [62].

While electrically insulating He has little effect on the magnitude of the magnetic field, the shallow slope $(\partial T/\partial P)_S$ of the hydrogen isentrope suggests the possibility that He has an important effect on convection and, thus, on the existence of the magnetic field. The criterion for convection to occur is $(\partial T/\partial P)_S\ (\partial T/\partial P) > [(\partial T/\partial P)_S]^2$, where $(\partial T/\partial P)$ is the actual variation of temperature with pressure in the planet. If $(\partial T/\partial P)_S > 0$, this becomes the usual Schwarzschild criterion. Since Jupiter has a magnetic field, $(\partial T/\partial P) > 0$ and thus $(\partial T/\partial P)_S > 0$, as well. Since for pure hydrogen $(\partial T/\partial P)_S \sim 0$ and might actually be slightly negative in the region of metallization, He might be necessary to make these derivatives positive for the Jovian hydrogen-He mixture. That is, if the hydrogen isentrope has a small negative slope in $(\partial T/\partial P)_S$ over an appreciable pressure (radius) range, temperature needs to increase only a few percent for this curve to have a positive slope everywhere. Unlike hydrogen, He has no internal degrees of freedom at the densities and temperatures in the envelop of Jupiter. Thus, He has a higher temperature than hydrogen at the same pressure and density. As a result, a relatively small concentration of He might be sufficient to make these derivatives positive. The hydrogen T-P curve in Fig. 11 suggests the speculation that relatively small fluctuations in He content over such an enormous planet might have a significant effect on the asymmetry of convection. At any rate, the asymmetric nature of the Jovian magnetic field might be caused by the shallow slope $(\partial T/\partial P)_S$ due to hydrogen dissociation, coupled with the He content.

The likely picture of the interior of Jupiter is illustrated in Fig. 12. The outermost layer contains molecular H_2. The continuous phase transition from H_2 to H commences at ~0.95 R_J. At ~0.90 R_J, 140 GPa, and ~4000 K hydrogen achieves the minimum conductivity of a metal. Semiconducting electrical conductivities at radii in the range 0.90-0.95 R_J might make significant contributions to the external magnetic field because of their proximity to the surface. Dissociation goes to completion, somewhere around 300 GPa. In the region above 140 GPa the conductivity

increases little from 2000 $(\Omega cm)^{-1}$ because of disorder in the fluid. Because of the continuous dissociative transition there is no distinct core-mantle boundary. The question of whether the transition from H_2 to H is first-order [48,63] or continuous [64] in Jupiter has been debated for years. A widely held view has been that a first-order transition from H_2 to H exists at the core-mantle boundary at 300 GPa, 10,000 K, and ~0.75 R_J. All the high-pressure fluid hydrogen experiments to date indicate that this transition is continuous. Because of the possible importance of He for convection, He might have an important effect on the magnetic field and its asymmetry. The possible importance of He for convection implies that He is soluable in fluid metallic hydrogen, contrary to the conventional expectation that metallic hydrogen and insulating He would phase separate. However, at ~100 GPa and ~4000 K, the question of their mutual solubility is yet to be resolved.

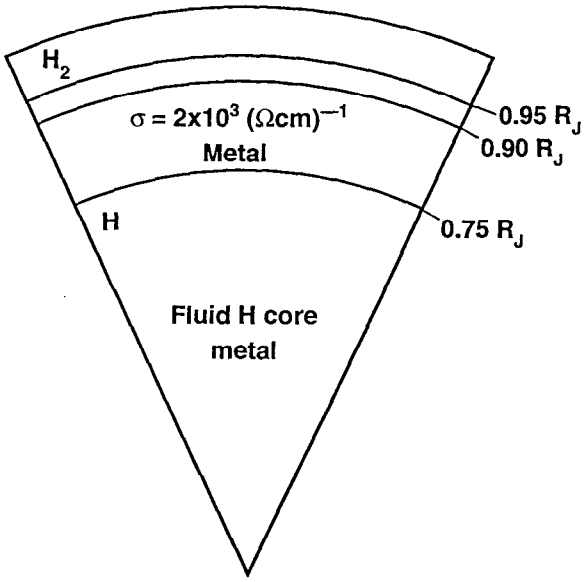

Fig. 12. Illustration of interior of Jupiter. For R > ~0.95 R_J, fluid hydrogen is molecular insulator. Between 0.95 R_J and 0.90 R_J fluid hydrogen is semiconducting and dissociates continuously with depth up to fraction of ~0.15 of original H_2 molecules [60]. At ~0.90 R_J fluid hydrogen reaches minimum metallic conductivity [61]. Dissociation is complete at ~0.75 R_J.

4b. Inertial Confinement Fusion

Experimental results for hydrogen are required to develop a more accurate EOS for hydrogen fuel at high pressures and temperatures encountered in ICF. That is, hydrogen at relevant high pressures and temperatures has thus far eluded theoretical understanding needed to develop the requisite EOS for optimum ICF design calculations. NIF is a giant laser now being built for ICF at an estimated cost of $1 B. In laser-driven ICF a fuel pellet composed of the hydrogen isotopes deuterium and tritium (DT) is placed in a hohlraum and radiated by a high-intensity laser pulse, multistepped in time [65]. The first step of the laser pulse produces a ~100 GPa shock and the successive pulses comprise a quasi-isentrope, similar to the compressive process used in the gas-gun conductivity experiments described above (Fig. 3). In order to achieve efficient nuclear-fusion reaction of DT, it is necessary to achieve the highest possible areal mass density. In order to maximize areal mass density, it is necessary to compress most of the DT fuel along an isentrope with minimal thermal pressure, that is, along a low-lying isentrope. This is accomplished by achieving maximum first-shock density with the lowest possible temperature.

Various isentropes and a Hugoniot of fluid DT are plotted as pressure versus density in Fig. 13 [65]. Figure 10 shows that the Hugoniot near 100 GPa is much more compressible than thought previously, as in Fig. 13. Figure 10 also shows that, because of the high compression on the Hugoniot, DT can be placed on a lower lying isentrope to get higher fusion energy yields from NIF, but only if the EOS of DT were known throughout this regime. However, Fig. 10 demonstrates that there is no general theoretical understanding of hydrogen in this regime, which is in the middle of a very complex continuous phase transition from solid to fluid, from insulator to metal, from diatomic to monatomic, and from quantum to classical.

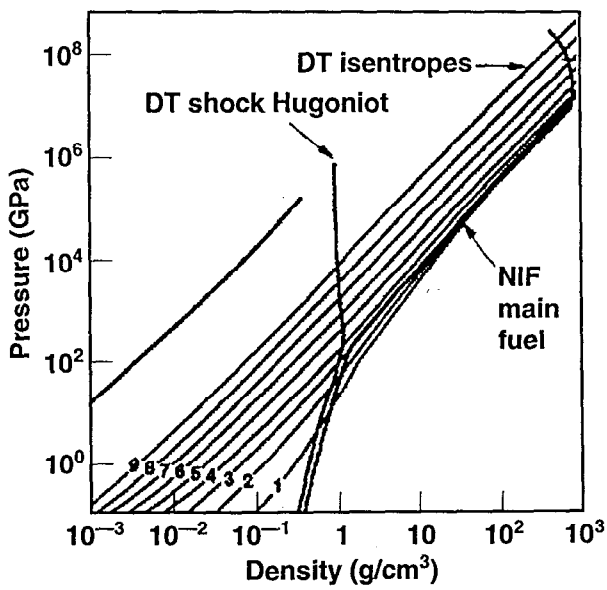

Fig. 13. Theoretical Hugoniot and several isentropes of DT plotted as pressure versus density [65].

Electrical conductivity experiments probe states which are essentially on isentropes starting on the Hugoniot (Fig. 1). The EOS of fluid DT in this regime depends on dissociation of molecules, via both internal energy absorbed and interactions between particles so formed, and on electronic excitation (ionization) because energy absorbed in this process does not produce thermal pressure. The importance to ICF stems from the fact that even though these processes occur near 100 GPa, they affect the isentrope along which DT is compressed (Fig. 13), which in turn affects the ultimate fusion energy yield generated at pressures orders of magnitude larger than 100 GPa. Further research on hydrogen at ~100 GPa and ~1 eV using a two-stage gun and giant lasers is required in

order to determine a more accurate EOS with which to design the most efficient ICF fuel capsules.

4c. Metastable Solid Metallic Hydrogen

It is not known how, nor even whether, metallic fluid hydrogen could be quenched to metastable solid metallic hydrogen (MSMH) at ambient pressure and temperature. However, the potential scientific and technological benefits are enormous if it could be [2]. A quenched fluid is a glass. Producing the metallic fluid by shock compression has the advantage that large quantities of glassy MSMH possibly might be made using large systems of explosives, as DuPont shock-synthesizes industrial diamond powders in a cylindrical system 4 m high and 1 m in diameter [66]. In this way it might be possible to take advantage of the fact that the disordered fluid is metallic at unexpectedly lower pressures (~100 GPa) than thought previously for the solid (~400 GPa).

MSMH has been predicted to be a room-temperature superconductor in both the monatomic [1] and diatomic [67] crystalline phases and might also superconduct in the dense glass phase, as well. In general, the electrical, magnetic, optical, thermal, and mechanical properties are expected to be very unusual for this novel quantum, metallic solid.

We also speculate that the degree of metastability of MSMH might be tuneable. Highly metastable MSMH might be useful as a light-weight structural material, provided it has strength. It might have strength because additives will probably be necessary for metastability. MSMH might also be a fuel, propellant, or explosive depending on the rate of release of stored energy, that is, on the degree of metastability.

Hydrogen in the form of DT is used as the fuel in laser-driven ICF. MSMH in the form of solid DT targets would produce substantially higher fusion yields than other forms of DT because of its high density. The extremely high density of metallic DT would mean that substantially more fuel could be packed into a given space than targets with gaseous or cryogenic molecular-solid fuel. In addition, high MSMH initial density might reduce the growth of hydrodynamic instabilities, which in turn would increase thermonuclear reaction efficiency. Thus, future giant lasers would have an even larger margin for success than expected previously.

The hydrogen phase diagram must be known to determine an optimal quenching system. That is, the probability of recovering material successfully increases inversely with shock pressure. Thus, it is important to know the lowest shock pressure and temperature required to reach the metallic state in order to maximize the probability of quenching MSMH in a successful shock recovery experiment. The phase diagram of hydrogen is illustrated schematically in Fig. 14 [9]. The metallization point measured in the fluid is the point at 140 GPa and 2600 K [5,7]. The triple point at 150 GPa of insulating solid phases I, II, and III was measured by Cui et al [68] and by Mao and Hemley [69]. The melt line was calculted by Ross et al [17]. The slope of the metallization curve is assumed to be negative because metallization pressure at 0 K is predicted to be about 300 GPa [19] and observed to be greater than 340 GPa at 300 K [27]. At sufficiently high temperatures hydrogen is completely dissociated and ionized to produce an electron/proton plasma.

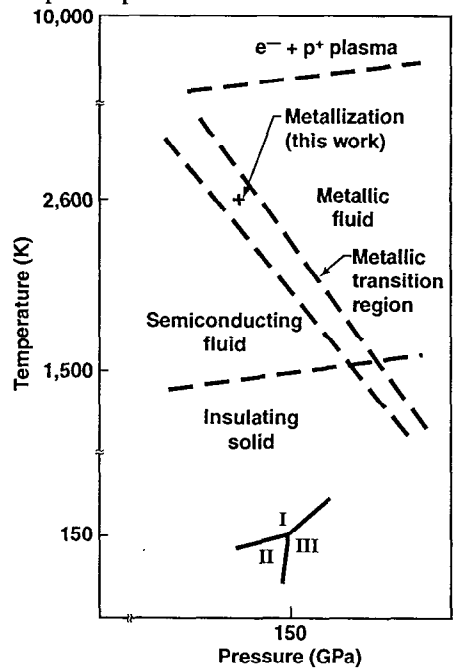

Fig. 14. Schematic hydrogen phase diagram [9]: + is metallization point observed by conductivity experiments in shock-compressed fluid [5]; triple point of solid phases I-III observed in optical experiments in diamond-anvil cells [68,69]; calculated melting curve [17]; and other estimated phase lines.

5. Acknowledgement

This work was performed under the auspices of the U. S. Department of Energy under Contract No. W-7405-ENG-48 by LLNL.

References

[1] N. W. Ashcroft, *Phys. Rev. Lett.*, **21**, 1748 (1968)
[2] W. J. Nellis, *Phil. Mag. B*, **79**, 655 (1999)
[3] T. W. Barbee III, A. Garcia, M. L. Cohen, J. L. Martins, *Phys. Rev. Lett.*, **62**, 1150 (1989)
[4] P. Loubeyre, R. LeToullec, D. Hausermann, M. Hanfland, R. J. Hemley, H. K. Mao, L. W. Finger, *Nature*, **383**, 702 (1996)
[5] S. T. Weir, A. C. Mitchell, W. J. Nellis, *Phys. Rev. Lett.*, **76**, 1860 (1996)
[6] L. B. Da Silva et al., *Phys. Rev. Lett.*, **78**, 483 (1997)
[7] W. J. Nellis, S. T. Weir, A. C. Mitchell, *Phys. Rev. B*, **59**, 3434 (1999)
[8] T. J. Lenosky, J. D. Kress, L. A. Collins, I. Kwon, *Phys. Rev. B*, **55**, R11,907 (1997)
[9] W. J. Nellis, A. A. Louis, N. W. Ashcroft, *Phil. Trans. R. Soc. Lond. A*, **356**, 119 (1998)
[10] K. Mendelssohn, *The Quest for Absolute Zero*, World University Library, New York, 1966, p. 64

[11] K. F. Herzfeld, *Phys. Rev.*, **29**, 701 (1927)
[12] P. P. Edwards, R. L. Johnston, C. N. R. Rao, D. P. Tunstall, and F. Hensel, *Phil. Trans. R. Soc. Lond. A*, **356**, 5 (1998)
[13] E. Wigner, H. B. Huntington, *J. Chem. Phys.*, **3**, 764 (1935)
[14] B. J. Alder, R. H. Christian, *Phys. Rev. Lett.*, **4**, 450 (1960)
[15] R. S. Hawke et al., *Phys. Rev. Lett.*, **41**, 994 (1978)
[16] K. Inoue, H. Kanzaki, S. Suga, *Solid State Commun.*, **30**, 627 (1979)
[17] M. Ross, F. H. Ree, D. A. Young, *J. Chem. Phys.*, **79**, 1487 (1983)
[18] A. I. Pavlovskii et al., *Megagauss Technology and Pulsed Power Applications*, edited by C. M. Fowler, R. S. Caird, D. J. Erickson, Plenum Press, New York, 1987, p. 255
[19] N. W. Ashcroft, *Phys. Rev. B*, **41**, 10963 (1990)
[20] H. K. Mao, P. M. Bell, R. J. Hemley, *Phys. Rev. Lett.*, **55**, 99 (1985)
[21] A. Garcia, T. W. Barbee, M. L. Cohen, I. F. Silvera, *Europhys. Lett.*, **13**, 355 (1990).
[22] H. Chacham, S. G. Louie, *Phys. Rev. Lett.*, **66**, 64 (1991)
[23] E. Kaxiras, J. Broughton, R. J. Hemley, *Phys. Rev. Lett.*, **67**, 1138 (1991)
[24] H. N. Chen, E. Sterer, I. F. Silvera, *Phys. Rev. Lett.*, **76**, 1663 (1996)
[25] R. J. Hemley, H. K. Mao, A. F. Goncharov, M. Hanfland, V. Struzhkin, *Phys. Rev. Lett.*, **76**, 1667 (1996).
[26] A. L. Ruoff, *High Pressure Science and Technology*, edited by W. Trzeciakowski, World Scientific, Singapore, 1996, p. 511
[27] C. Narayana, H. Luo, J. Orloff, A. L. Ruoff, *Nature*, **393**, 46 (1998)
[28] V. E. Fortov et al., *Bull. Am. Phys. Soc.*, **42**, 1494 (1997); V. Ya. Ternovoi et al., *Physica B*, **265**, 6 (1999)
[29] F. Hensel, P. Edwards, *Phys. World*, **April**, 43 (1996)
[30] T. W. Barbee III, LLNL, private communication (1996)
[31] N. F. Mott and E. A. Davis, *Electronic Processes in Non-Crystalline Materials*, Oxford University Press, London, 1971
[32] V. V. Brazhkin, S. V. Popova, R. N. Voloshin, A. G. Umnov, *High Pressure Res.*, **6**, 363 (1992)
[33] B. M. Riggleman, H. G. Drickamer, *J. Chem. Phys.*, **38**, 2721 (1963)
[34] R. J. Hemley, N. W. Ashcroft, *Phys. Today*, **August**, 26 (1998)
[35] N. C. Holmes, M. Ross, W. J. Nellis, *Phys. Rev. B*, **52**, 15835 (1995).
[36] T. J. Lenosky, J. D. Kress, L. A. Collins, I. Kwon, *Phys. Rev. B*, **55**, R11907 (1997)
[37] J. Kress, L. Collins, T. Lenosky, I. Kwon, N. Troullier, *Strongly Coupled Coulomb Systems*, Plenum Press, New York, 1998, p. 331.
[38] N. W. Ashcroft, Phys. World, **8**, 43 (1995); B. Edwards, N. W. Ashcroft, *Nature*, **388**, 652 (1997)
[39] R. Chau, A. C. Mitchell, R. Minich, W. J. Nellis, this proceedings
[40] R. Chau et al., submitted (1999)
[41] M. Bastea, A. C. Mitchell, W. J. Nellis, this proceedings
[42] R. C. Dynes, J. M. Rowell, P. H. Schmidt, *Ternary Superconductors*, edited by G. K. Shenoy, B. D. Dunlap, F. Y. Fradin, Elsevier, Amsterdam, 1981, p. 169
[43] G. W. Collins et al., *Science*, **281**, 1178 (1998)
[44] W. J. Nellis et al., *J. Chem. Phys.*, **79**, 1480 (1983)
[45] M. Ross, *Phys. Rev. B*, **58**, 669 (1998)
[46] G. I. Kerley, *J. Chem. Phys.*, **73**, 460 (1980)
[47] W. R. Magro, D. M. Ceperley, C. Pierleoni, B. Bernu, *Phys. Rev. Lett.*, **76**, 1240 (1996)
[48] D. Saumon, G. Chabrier, *Phys. Rev. A*, **46**, 2084 (1992)
[49] T. J. Lenosky, J. D. Kress, L. A. Collins, *Phys. Rev. B*, **56**, 5164 (1997)
[50] D. Beule, W. Ebeling, A. Forster, H. Juranek, R. Redmer, G. Ropke, *Contrib. Plas. Phys.*, **39**, 21 (1999)
[51] G. W. Collins et al., submitted (1999)
[52] P. Celliers et al., Lawrence Livermore National Laboratory Report UCRL-JC-130339-REV-1, (1999)
[53] W. B. Hubbard, *Science*, **214**, 145 (1980)
[54] D. J. Stevenson, *Annu. Rev. Earth Planet. Sci.*, **10**, 257 (1982)
[55] V. N. Zharkov, T. V. Gudkova, *High-Pressure Research: Application to Earth and Planetary Sciences*, edited by Y. Syono, M. H. Manghnani, Terra Scientific Publishing, Tokyo, 1992, p. 393
[56] M. Ross, H. C. Graboske, W. J. Nellis, *Phil. Trans. R. Soc. Lond. A*, **303**, 303 (1981)
[57] D. J. Stevenson, *Rep. Prog. Phys.*, **46**, 555 (1983)
[58] E. J. Smith, L. Davis, D. E. Jones, *Jupiter*, edited by T. Gehrels, University of Arizona Press, Tucson, 1976, p. 788
[59] M. H. Acuna, N. F. Ness, *J. Geophys. Res.*, **81**, 2917 (1976)
[60] W. J. Nellis, M. Ross, N. C. Holmes, *Science*, **269**, 1249 (1995)
[61] W. J. Nellis, S. T. Weir, A. C. Mitchell, *Science*, **273**, 936 (1996)
[62] W. J. Nellis, *Planetary and Space Sci.* (in press)
[63] D. J. Stevenson, E. E. Salpeter, *Astrophys. J. Suppl. Ser.*, **35**, 221 (1977)
[64] W. B. Hubbard, M. S. Marley, *Icarus*, **78**, 102 (1989)
[65] J. Lindl, *Phys. Plasmas*, **2**, 3933 (1995)
[66] O. R. Bergmann, *Shock Waves in Condensed Matter-1983*, edited by J. R. Asay, R. A. Graham, G. K. Straub, Elsevier Press, Amsterdam, 1984, p. 429
[67] C. F. Richardson, N. W. Ashcroft, *Phys. Rev. Lett.*, **78**, 118 (1997)
[68] L. Cui, N. H. Chen, S. J. Jeon, I. F. Silvera, *Phys. Rev. Lett.*, **72**, 3048 (1994)
[69] H. K. Mao, R. J. Hemley, *Rev. Mod. Phys.*, **66**, 671 (1994)